

## Review article

## A review on laser deposition-additive manufacturing of ceramics and ceramic reinforced metal matrix composites



Yingbin Hu, Weilong Cong\*

Department of Industrial, Manufacturing, and Systems Engineering, Texas Tech University, Lubbock, TX 79409-3061, USA

## ARTICLE INFO

**Keywords:**  
 B. Composites  
 B. Defects  
 C. Mechanical properties  
 D. Traditional ceramics  
 Laser deposition-additive manufacturing

## ABSTRACT

Ceramics and ceramic reinforced metal matrix composites (MMCs) are widely used in severe working conditions and have been applied in biomedical, aerospace, electronic, and other high-end engineering industries owing to their superior properties of high wear resistance, outstanding chemical inertness, and excellent properties at elevated temperatures. These superior properties, on the other hand, make it difficult to process these materials with conventional manufacturing methods, posing problems of high cost and energy consumptions. In response to this problem, direct additive manufacturing (AM), which is equipped with a high-power-density laser beam as heat source, has been developed and extensively employed for processing ceramics and ceramic reinforced MMCs. Compared with other direct AM processes, laser deposition-additive manufacturing (LD-AM) process excels in several aspects, such as lower labor intensity, higher fabrication efficiency, and capabilities of parts remanufacturing and functionally gradient composite materials fabrication. Besides these benefits, problems of poor bonding, cracking, lowered toughness, etc. still exist in LD-AM fabricated parts. This paper reviews developments on LD-AM of ceramics and ceramic reinforced MMCs in both bulk parts fabrication and cladding. Main issues to be solved, corresponding solutions, and the trend of development are summarized and discussed.

## 1. Introduction

Ceramics and ceramic reinforced metal matrix composites (MMCs) demonstrate superior properties of high modulus and strength, good wear resistance, outstanding chemical inertness, and excellent properties at elevated temperatures [1–4]. Owing to the benefits exhibited, ceramics and ceramic reinforced MMCs have been widely used in severe working conditions (e.g. high-load condition, high-wear/friction condition, high-temperature condition, etc. [3,5,6]) and gain their popularity in many commercial applications, including biomedical (e.g. acetabular cups, dental restoration frameworks, etc. [7,8]), aerospace (e.g. engine components, heat-resistant tiles, etc. [9]), electronic (e.g. insulators, transducers, etc. [10]) and other high-end engineering (e.g. machining tools, bearing components, etc. [11,12]) industries.

Because of their high hardness and high melting point, ceramics and ceramic reinforced MMCs are difficult to process by conventional manufacturing methods [13–16]. Zhang et al. published a work on diamond grinding of hot-pressed  $\text{Si}_3\text{N}_4$ , hot-pressed  $\text{Al}_2\text{O}_3$ , slip-casted  $\text{ZrO}_2$ , and sintered  $\text{SiC}$  ceramics [16]. Hot-pressing, slip-casting, and sintering caused high cost and energy consumptions. In addition, damages of pulverization and microcracking were induced by grinding. With increased competitiveness, additive manufacturing (AM) has

attracted a great deal of attentions and is under intensive investigations for fabricating ceramics and ceramic reinforced MMCs [1,2,4,17–32]. AM is described by the American Society for Testing and Materials (ASTM) as “a process of joining materials to make objects from 3D model data, usually layer upon layer, as opposed to subtractive manufacturing technologies” [33]. Compared with conventional manufacturing methods, AM has extended capability of fabricating complex-shaped parts and benefits of high design flexibility, high customization, shortened lead time, no need of assembly or molds, lowered energy use, etc. [34,35].

Table 1 provides a summary of AM processes for fabricating ceramics and ceramic reinforced MMCs. It can be seen that AM mainly includes indirect AM method and direct AM method. In indirect AM method (e.g. fused deposition modeling (FDM), stereolithography (SLA), direct inkjet printing (DIP), layer-wise slurry deposition (LSD), laminated object manufacturing (LOM), etc.), preliminary 3D structures (green bodies) are built with binder materials. Afterwards, the green bodies are sintered to eliminate the binder materials and densified by conventional manufacturing processes. Different from indirect AM method, direct AM method combines the forming and densification procedures and generates final components without post-sintering process. Therefore, direct AM method can produce components with

\* Corresponding author.

E-mail address: [weilong.cong@ttu.edu](mailto:weilong.cong@ttu.edu) (W. Cong).

**Table 1**

AM processes for fabricating ceramics and ceramic reinforced MMCs.

Process	Type of starting material	Layer creation technique	Ceramic/Ceramic reinforced MMC	Refs.
Indirect	FDM	Filament	Material extrusion	[17]
	SLA	Photocurable resin and powders	Photo curing by laser scanning	[18]
	DIP	Powder suspension	Inkjet printing	[19–21]
	LSD	Slurry	Slurry deposition	[22]
	LOM	Sheet	Sheeting binding and laser cutting	[23]
Direct	Direct SLS	Powder in bed	Partially melted by laser scanning	[24]
	SLM	Powder in bed	Fully melted by laser scanning	[25]
	LD-AM	Powder injected through nozzle	Laser deposition	[26]
			Ceramic	[27]
			Ceramic reinforced MMC	[28]
			Ceramic	[29]
			Ceramic reinforced MMC	[30]
			Ceramic	[1,2,31]
			Ceramic reinforced MMC	[4,32]

relatively higher density, higher purity, better mechanical properties, less energy- and time-consuming, as compared with indirect AM method [36,37]. In addition, direct AM method uses a laser as heat source and the laser has high directionality and high energy intensity and can deliver a great amount of energy to a micro-scale focal region, being capable of processing a wide range of materials [38].

Direct selective laser sintering (direct SLS) used to be a dominant direct AM process in fabrication of ceramics and ceramic reinforced MMCs [27,28]. However, due to the fact that direct SLS can only partially melt starting powders and fabricated parts have low density and poor mechanical properties, the applications of direct SLS are restricted. To meet the requirement of producing near-full-dense parts with better mechanical properties, selective laser melting (SLM), which can fully melt starting powders, has been developed [39]. A schematic illustration of direct SLS and SLM is shown in Fig. 1. At first, the substrate is driven downward by a mounted build piston, leaving one-layer-thickness space. Then, a powder distributor doses a certain amount of powder and evenly spreads the supplied powder on the substrate to fill the space. The generated laser beam, which is controlled and directed by X-Y scanning mirrors and an f-θ lens, selectively melts the powder and forms the first layer. Afterwards, the substrate descends another layer

thickness for the next layer creation. Layer upon layer, the designed near-net-shape component will be fabricated by repeating these steps [40].

In comparison with powder-bed based direct SLS and SLM processes, laser deposition-additive manufacturing (LD-AM, mainly including laser engineered net shaping (LENS) and direct metal deposition (DMD)) process possesses advantages of lower labor intensity and higher fabrication efficiency and shows capabilities of parts remanufacturing and functionally gradient composite (FGC) materials fabrication [41–43]. Fig. 2 shows a part being repaired by LENS process [44]. Besides these benefits, problems of poor bonding, cracking, lowered toughness, etc. exist in LD-AM of ceramics and ceramic reinforced MMCs [2,4,45]. For the purpose of reducing or solving the problems mentioned above, researchers have been dedicated to understanding formation mechanisms of these problems and seeking solutions to them. The solutions include (but are not limited to) optimizing process parameters, adding a buffer layer/FGC layers, integrating with assisting technology of ultrasonic vibration, pre-/post-heating, adding additive materials, tailoring novel microstructure, etc. [1,2,4,31,42,46–62]. This paper reviews developments on LD-AM of ceramics and ceramic reinforced MMCs. In addition, main issues to be solved, corresponding solutions, and the trend of development are also discussed.

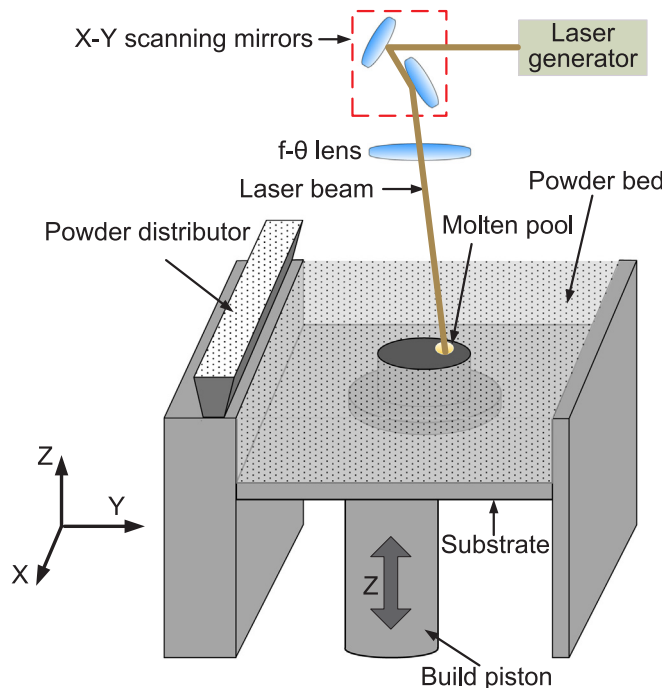


Fig. 1. Schematic illustration of direct SLS and SLM processes.

## 2. Laser deposition-additive manufacturing process

Fig. 3 shows the schematic illustration of LD-AM process. At the beginning, the substrate is selectively melted by heat from laser radiation, forming a molten pool which catches and melts powders supplied by a powder stream. When the laser beam moves away, the molten pool starts to solidify as a consequence of heat dissipation. The deposition head moves along the designed trajectory based on a 3D file, forming the first layer on the substrate. Afterwards, the deposition head

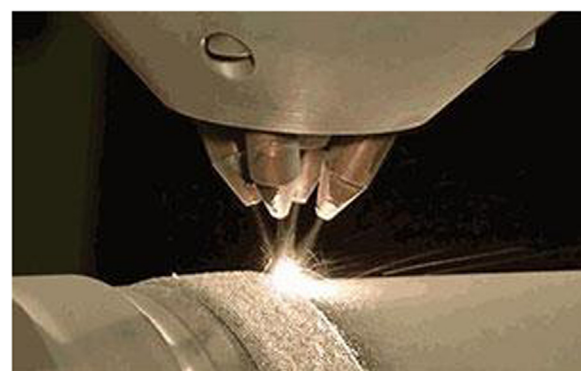


Fig. 2. Part repair using LENS [44]. (Photo courtesy of Optomec Inc.).

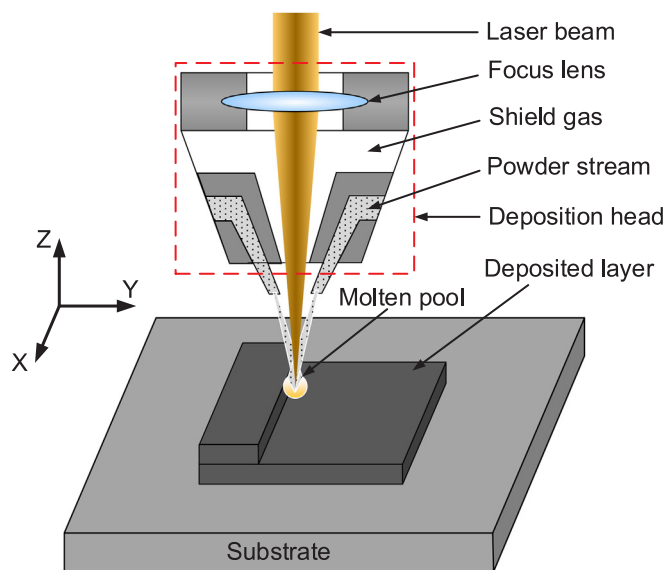


Fig. 3. Schematic illustration of LD-AM process.

ascends one layer thickness to a new set position for the next layer deposition. Served as the new “substrate”, the first layer is partially melted with the formation of the second layer. Similar steps will be repeated many times until the designed near-net-shape component is built layer by layer [36].

In LD-AM process, part quality depends on energy input which can be controlled via changing process parameters of laser power, scanning speed, hatch distance, and powder feeding rate [63]. Besides energy input, layer thickness will also be determined by these process parameters. It is of great importance to set layer thickness as Z-axis increment since the mismatch between layer thickness and Z-axis increment will impair energy utilization and negatively affect dimensional

accuracy along Z direction, thus resulting in poor part quality (such as low density [64]) or even failure of part fabrication. As shown in Fig. 4, if the Z-axis increment value equals the layer thickness (Case 1), the focal point will be on the top surface of each layer and the layer thickness will be uniform. After fabrication of the first layer, if the focal point is above the top surface (Case 2), the laser energy input will be weakened, generating a thinner second layer. The distance between the focal point and the top surface of the second layer will be even further, generating even thinner third layer. The layers fabricated will be thinner and thinner until nothing will be further fabricated. After fabrication of the first layer, if the focal point is below the top surface (Case 3), the laser energy input will be reduced, generating a thinner second layer, comparing with the first layer. Then, the distance between the top surface of the second layer and the focal point will be smaller and then a thicker third layer is generated, in comparison with the second layer. Based on analysis, it can be concluded that Case 1 is the ideal case which exhibits following advantages: (1) The layer thickness is uniform and the build height can be expected; (2) The laser energy input for each layer is stable, rendering uniform properties of fabricated layers; (3) The laser energy can be efficiently and effectively utilized.

Within each layer, there are four common scanning patterns, including raster, offset from inside to outside, offset from outside to inside, and fractal patterns, as shown in Fig. 5(a)–(d) [65]. Yu et al. conducted research on effects of scanning patterns on part distortion and part quality in LD-AM process. Results showed that the offset from outside to inside and fractal patterns generated smaller thermal gradient, smaller substrate deformation, and better part quality, as compared with raster and offset from inside to outside patterns. For multiple layers, Hu et al. reported a zigzag scanning pattern with 90° orientation changing for each layer, as shown in Fig. 5(e) [36]. Such scanning pattern could attenuate side effects of high thermal stress and part distortion induced by scanning orientation.

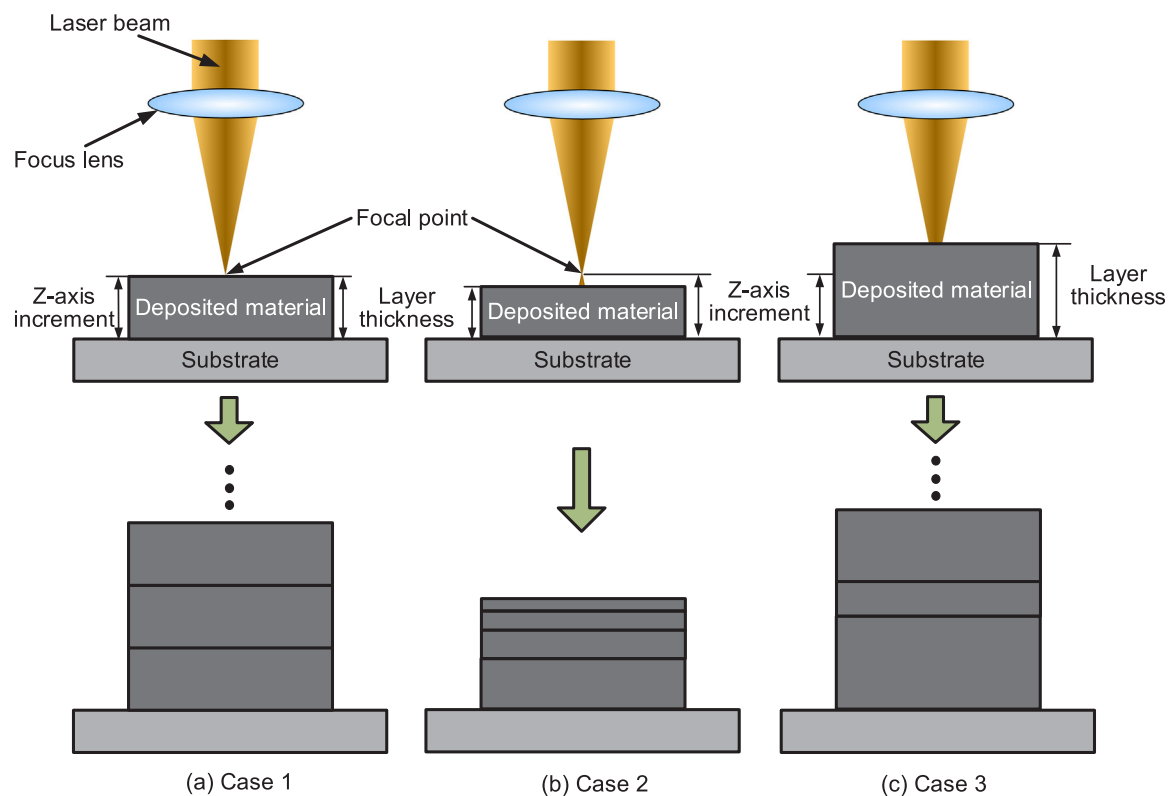
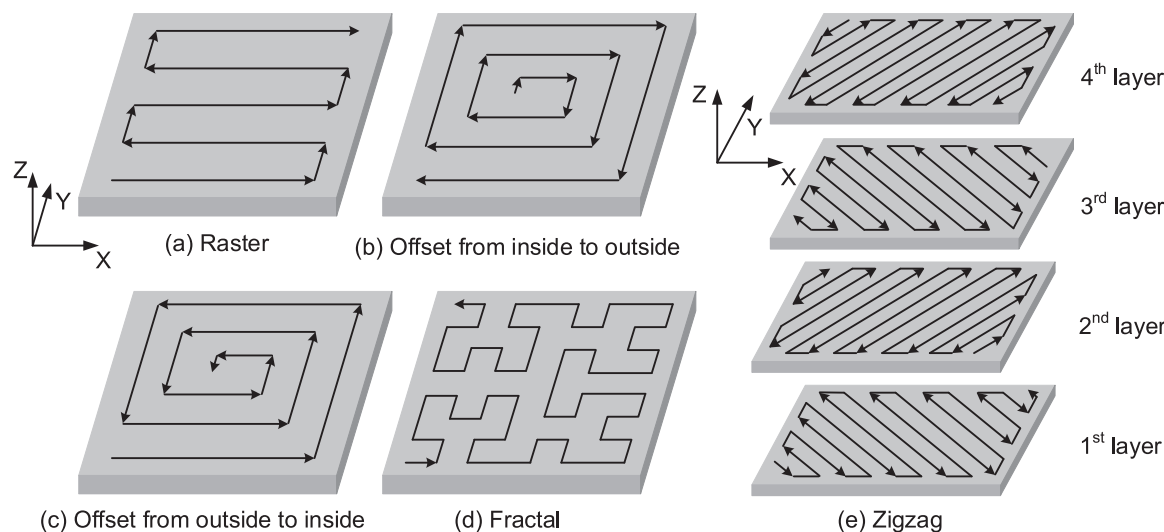


Fig. 4. Effects of relationship between Z-axis increment and layer thickness in LD-AM process.



**Fig. 5.** (a) Raster, (b) offset from inside to outside, (c) offset from outside to inside, and (d) fractal scanning patterns within one layer and (e) zigzag scanning pattern for multiple layers.

### 3. Bulk parts fabrication by laser deposition

On account of the capability of depositing multiple layers, LD-AM demonstrates its feasibility of producing near-net-shape parts.

#### 3.1. Ceramics

Equipped with high-power-density laser beams, LD-AM process finds applications in processing high hardness and high-melting-point (up to 3000 °C) ceramics, such as Al<sub>2</sub>O<sub>3</sub> and ZrO<sub>2</sub>-Al<sub>2</sub>O<sub>3</sub> [1,31,52,59,66]. A summary on ceramics fabricated by LD-AM process is provided in Table 2.

##### 3.1.1. Al<sub>2</sub>O<sub>3</sub> ceramics

Balla et al. successfully fabricated dense and net-shaped structures (e.g. cylinder, cube, gear, etc.) of Al<sub>2</sub>O<sub>3</sub> by LD-AM process [31]. Experimental results showed that columnar grains formed along the build direction and fabricated parts exhibited anisotropy in mechanical properties. In Li et al.'s work, process parameters of laser power, scanning speed, and powder feeding rate were varied to shed light on their effects on deposition qualities (including dimensions, surface roughness, flatness, powder efficiency, and microhardness) in LD-AM of Al<sub>2</sub>O<sub>3</sub> [37]. Besides deposition qualities, Wu et al. reported that different process parameters of LD-AM resulted in different colors (white/black) of fabricated Al<sub>2</sub>O<sub>3</sub> thin-wall structures [67]. Table 3 shows the chemical composition of Al<sub>2</sub>O<sub>3</sub> powder used in that investigation. According to analysis, the essential reason for the black appearance was the generation of second Ca-β-Al<sub>2</sub>O<sub>3</sub>, NaAl<sub>6</sub>O<sub>9.5</sub>, and CaAl<sub>2</sub>Si<sub>2</sub>O<sub>8</sub> phases and unmelted Al<sub>2</sub>O<sub>3</sub> particles under low energy input. The emergence of these second phases would give rise to the formation and propagation of inner defects and increase volatility degree of oxide impurities, amount of encaptured gas, and shrinkage differences, thus resulting in the black color. The authors also found that dense and evenly-distributed cracks were presented on the surfaces of black structure and grew along the build direction. Compared with the black structure, the white structure contained much fewer cracks, which were mainly on the top portion of surfaces. Aiming at acquiring desired part qualities and properties, process parameters of LD-AM should be optimized. To avoid tremendous experiments for finding optimal process parameters, a mathematical model, which could reveal the relationship between process parameters and physical properties of fabricated Al<sub>2</sub>O<sub>3</sub> parts, was developed by Niu et al. [52].

**Table 2**  
Summary of ceramics fabricated by LD-AM process.

	Particle size (μm)	Process parameters	Refs.
Al <sub>2</sub> O <sub>3</sub>	Al <sub>2</sub> O <sub>3</sub> : 44–74	Laser power (W): 175 Scanning speed (mm/s): 10.00 Powder feeding rate (g/s): 0.230	[31]
	Al <sub>2</sub> O <sub>3</sub> : 40–80	Laser power (W): 175–250 Scanning speed (mm/s): 8.33–25.00	[37]
	Al <sub>2</sub> O <sub>3</sub> : 42–90	Laser power (W): 175–298; 398–520 Scanning speed (mm/s): 5.00–8.33; 6.67–8.67; 18.33–21.67 Powder feeding rate (g/s): 0.020–0.023; 0.033–0.047 Z-axis increment (mm): 0.05; 0.15	[67]
	Al <sub>2</sub> O <sub>3</sub> : 42–90	Laser power (W): 230; 255; 326; 410; 510 Scanning speed (mm/s): 5.00 Powder feeding rate (g/s): 0.023	[52]
ZrO <sub>2</sub> -Al <sub>2</sub> O <sub>3</sub>	ZrO <sub>2</sub> & Al <sub>2</sub> O <sub>3</sub> : 42–90	Laser power (W): 410 Scanning speed (mm/s): 6.67 Powder feeding rate (g/s): 0.020 (Al <sub>2</sub> O <sub>3</sub> ); 0.015 (ZrO <sub>2</sub> ) Z-axis increment (mm): 0.25	[1]
	ZrO <sub>2</sub> & Al <sub>2</sub> O <sub>3</sub> : 40–90	Laser power (W): 360 Scanning speed (mm/s): 6.33 Powder feeding rate (g/s): 0.027 Z-axis increment (mm): 0.22	[61]
	ZrO <sub>2</sub> : 1–5; Al <sub>2</sub> O <sub>3</sub> : 45–75	Laser power (W): 325; 350; 375; 400 Scanning speed (mm/s): 10.00 Powder feeding rate (g/s): 0.033 Z-axis increment (mm): 0.51	[2]
PZT	PTZ: 50–150	Laser power (W): 150; 200; 250; 300 Scanning speed (mm/s): 5.00–10.00; 15.00 Powder feeding rate (g/s): 0.022; 0.033; 0.050	[72]

**Table 3**  
Chemical composition of Al<sub>2</sub>O<sub>3</sub> powder.

Chemical composition	Al <sub>2</sub> O <sub>3</sub>	Na <sub>2</sub> O	Fe <sub>2</sub> O <sub>3</sub>	SiO <sub>2</sub>	Cao
wt%	99.732	0.110	0.068	0.056	0.034

##### 3.1.2. ZrO<sub>2</sub>-Al<sub>2</sub>O<sub>3</sub> and other ceramics

Zirconia-alumina (ZrO<sub>2</sub>-Al<sub>2</sub>O<sub>3</sub>) excels pure Al<sub>2</sub>O<sub>3</sub> in several aspects, including enhanced toughness, superior properties of excellent

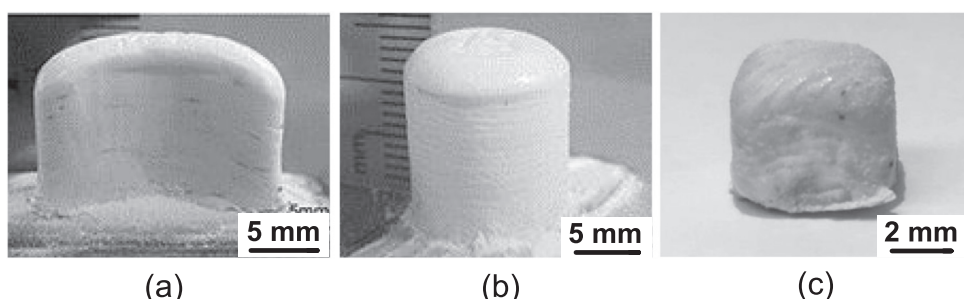


**Fig. 6.** LD-AM fabricated ZrO<sub>2</sub>-Al<sub>2</sub>O<sub>3</sub> parts with different shapes: (a) Arc wall [59]; (b) Cylinder [59]; and (c) Cube [2]. (Reprinted from Ref. [59], copyright (2015), with permission from Emerald Publishing Limited; Reprinted from Ref. [2], copyright (2018), with permission from Elsevier).

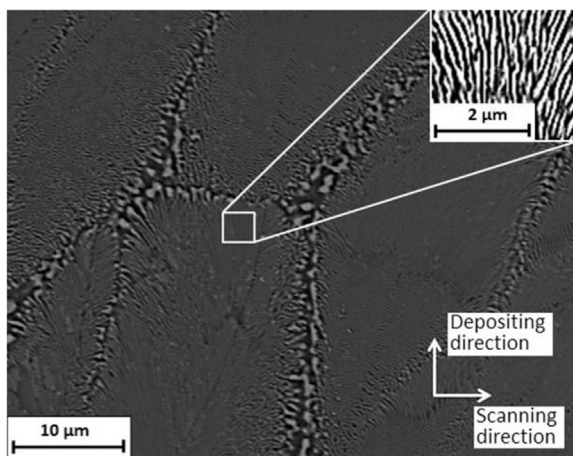


**Fig. 7.** Eutectic microstructure of a LD-AM fabricated ZrO<sub>2</sub>-Al<sub>2</sub>O<sub>3</sub> part [52]. (Reprinted from Ref. [1], copyright (2015), with permission from Elsevier).

corrosion and thermal resistances, good biocompatibility, and controllable mechanical properties via changing ZrO<sub>2</sub> content and powder preparation parameters [2,68–70]. Because of these strengths, ZrO<sub>2</sub>-Al<sub>2</sub>O<sub>3</sub> gains its popularity among researchers and has been widely used in many commercial applications, including biomedical (e.g. orthopaedic parts [68], dental components [71], etc.), chemical (e.g. valve seats, tubes [69], etc.), and high-end engineering (e.g. machining tools [11], bearing components [12], etc.) industries. Fig. 6 shows LD-AM fabricated ZrO<sub>2</sub>-Al<sub>2</sub>O<sub>3</sub> parts with arc-wall, cylindrical, and cubic shapes [2,59]. Niu et al. successfully fabricated cylindrical and arc-shaped ZrO<sub>2</sub>-Al<sub>2</sub>O<sub>3</sub> eutectic microstructure by LD-AM process using pure ZrO<sub>2</sub> and Al<sub>2</sub>O<sub>3</sub> powders with an eutectic ratio of 41.5 wt%: 58.5 wt% [1]. Due to the rapid melting/solidification process of LD-AM, a fine-grained microstructure with eutectic spacing of 100 nm was formed, as shown in Fig. 7. Such microstructure was reported to be refined and uniformized by introducing ultrasonic vibration to LD-AM process [61]. Compared with parts fabricated by LD-AM without ultrasonic vibration, parts fabricated by LD-AM with ultrasonic vibration showed improved mechanical properties. Using ultrasonic vibration-assisted LD-AM process, Hu et al. fabricated ZrO<sub>2</sub>-Al<sub>2</sub>O<sub>3</sub> bulk parts with a weight ratio of 10 wt%: 90 wt% between ZrO<sub>2</sub> and Al<sub>2</sub>O<sub>3</sub> [2]. The effects of ultrasonic vibration on microstructure and mechanical properties were analyzed, showing that the introduction of ultrasonic vibration helped to reduce grain size and improve microhardness, wear resistance, and compressive properties.

Besides Al<sub>2</sub>O<sub>3</sub> and ZrO<sub>2</sub>-Al<sub>2</sub>O<sub>3</sub>, LD-AM process was reported for fabrication of bulk lead zirconate titanate (PZT) ceramic parts. Results showed that desired dielectric properties were obtained, therefore, LD-AM process demonstrated its potential application in fabricating structural components of PZT based sensors and transducers [72].

### 3.2. Ceramic reinforced MMCs

Ceramic reinforced MMCs are made from no less than two types of materials (e.g. ceramics, non-metals, metals, alloys, etc.). In LD-AM process, these materials are either premixed using ball milling machine (option 1) or mixed from powder feeders (option 2). For option 2, the weight ratio between different materials can be controlled via regulating feeding rate of each powder feeder. Table 4 provides a summary on ceramic reinforced MMCs fabricated by LD-AM process.

#### 3.2.1. Ti-based composites

By reason of their high strength-to-weight ratio and excellent biocompatibility, ceramic reinforced titanium matrix composites (TMCs) have been widely applied in aeronautical and biomedical industries. In TMCs, ceramic reinforcement materials mainly include TiC [73,74], TiN [32], TiB [64], etc. Liu et al. successfully fabricated TiC reinforced TMCs using LD-AM process and studied effects of TiC content on microstructure and tensile properties [73]. Compared with Ti alloy, TMC with 5 vol% TiC exhibited better ultimate tensile strength (UTS) but worse ductility. With TiC content increasing from 5 vol% to 15 vol%, both UTS and ductility of TMCs were dramatically deteriorated. Borkar et al. introduced nitrogen to LD-AM process and formed TiN reinforcement. The in situ reacted TiN reinforcement homogeneously distributed throughout the Ti-Mo (90 wt%: 10 wt%) matrix [32]. Via changing the ratio between nitrogen and argon gases, the nitrogen content was tuned. Among all types of ceramic materials, in situ reacted TiB is considered as one of the most suitable ceramic reinforcements for TMCs allowing for following reasons: (1) Adding a small amount of TiB will hugely improve mechanical properties of TMCs; (2) Thermal stresses at interfaces of TiB and Ti can be minimized because of their similar densities and thermal expansion coefficients; (3) TiB is a stable phase and there is no intermediate phase between TiB and Ti; (4) The in situ process enables metallurgical bonding between TiB and Ti; (5) TiB is biocompatible and favors biomedical applications of TMCs [4,36,64,75]. Fig. 8(a) shows a typical microstructure of in situ synthesized TiB in LD-AM fabricated TMC [64]. The TiB exhibited B27

**Table 4**  
Summary of ceramic reinforced MMCs fabricated by LD-AM process.

	Materials used	Ceramic reinforcement	Metal matrix	Refs.
Ti-based	TA15, TiC	TiC	Ti matrix	[73]
	Ti6Al4V, TiC	TiC	Ti matrix	[74]
	Ti-Mo, N <sub>2</sub>	TiN	Ti-Mo matrix	[32]
	Ti, B	TiB	Ti matrix	[64]
Others	Ni, Ti, Ni coated graphite	TiC	Ni matrix	[79]
	TiC, IN625	TiC	IN625 matrix	[80]
	Invar, TiC	TiC	Invar	[81]

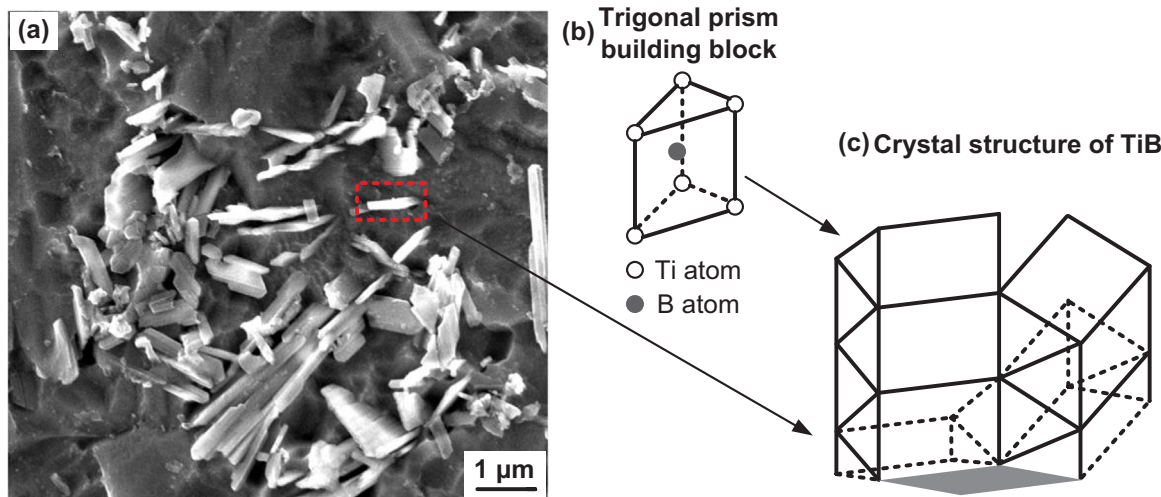


**Fig. 8.** TiB growth: (a) Scanning electron microscope (SEM) image of cross-sectional TiB reinforcement; Schematic illustration of (b) trigonal prism building block and (c) crystal structure of TiB. (Reprinted from Ref. [64], copyright (2017), with permission from Springer).

structure and formed a long prismatic shape with a high aspect ratio [76]. The formation mechanism of such a shape was studied by Lu et al. [77]. As shown in Fig. 8(b), a B atom located at the center of a trigonal prism building block with six Ti atoms at vertexes. The trigonal prism building blocks stacked in columnar arrays, sharing two of their rectangular faces with neighboring prisms along the B27[010] direction (in Fig. 8(c)) [76,77]. Based on the “Periodic Bond Chain” theory, TiB grains grew faster along [010] direction than along any other direction, forming the long prismatic shape [77,78].

### 3.2.2. Other composites

Ceramic reinforced Ni matrix composites (NMCs, in possession of high corrosion resistance and high fatigue resistance of Ni matrix as well as high hardness and high wear resistance of ceramic reinforcement) are considered as promising materials in a wide range of applications, such as aerospace, chemical, and petrochemical industries [79]. Hong et al. fabricated TiC reinforced NMCs using LD-AM process and proved that the presence of TiC reinforcement was to the benefit of refining grain size, as shown in Fig. 9 [80]. Compared with parts without reinforcement, the average grain size of TiC reinforced NMCs

was hugely reduced from 34.1 μm to 27.2 μm. In the investigation, effects of energy input per unit length on microstructure and mechanical properties (including wear and tensile properties) were studied. Results showed that high energy input led to efficient Marangoni convection within the molten pool and then refined and homogenized dispersion of TiC reinforcement, thus achieving enhanced wear and tensile properties. However, too high the energy input per unit length would coarsen columnar dendrites of the Ni matrix and weaken wear and tensile properties of NMCs.

As a rapid solidification process, LD-AM generates high temperature gradient and high thermal stress within fabricated parts and bring about defects of cracks, warpage, and even delamination. The use of Invar, which had low coefficient of thermal expansion (CTE), was reported to be an effective solution to such an issue [81]. Li et al. fabricated TiC reinforced Invar (64 wt% Fe + 36 wt% Ni) matrix composites (IMCs) using LD-AM process [81]. Experimental results showed that TiC reinforced IMCs had low CTE, high hardness, and high yield strength.

## 4. Laser cladding

Surface modification is the act of modifying the surface of a bulk material with purposes of enhancing surface properties or bringing biological or chemical characteristics to the material. These materials can be used for fabrication of specific products, such as load bearing implants, heat exchanger tubes, and coal slurry pipelines [3,5,6]. In the meantime, surface modification will not change bulk properties of the material. By virtue of the directionality and high energy density of its laser source, LD-AM of thin layers (known as laser cladding) is considered as an effective and efficient surface modification method [82]. In addition, a minimized heat input size leads to a small heat affected zone and low distortion of the bulk material [83].

### 4.1. Ceramics

#### 4.1.1. High wear performance applications

Cladding ceramics is proved to be resultful for enhancing wear resistance of materials those will be subject to rigorous friction conditions. Wang et al. laser cladded self-lubrication CaF<sub>2</sub>/Al<sub>2</sub>O<sub>3</sub> ceramic on Al<sub>2</sub>O<sub>3</sub> substrate using mixed CaF<sub>2</sub> and Al<sub>2</sub>O<sub>3</sub> powders by LD-AM process [55]. A scanning electron microscope (SEM) image of deposited layers (in Fig. 10) showed that spherical CaF<sub>2</sub> particles were uniformly dispersed in inter-plate regions of Al<sub>2</sub>O<sub>3</sub> matrix. The solid lubricating phase of CaF<sub>2</sub> had noticeably low friction coefficient and brought about significant enhancements in self-lubricating and wear resistance of

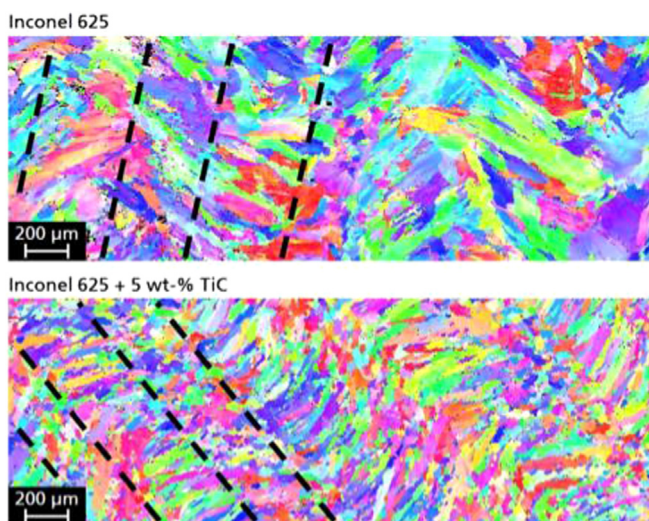


**Fig. 9.** Electron backscatter diffraction micrographs showing crystal structure characterizations of LD-AM fabricated Inconel 625 and TiC reinforced Inconel 625 matrix composite parts [80]. (Reprinted from Ref. [80], copyright (2015), with permission from Elsevier).

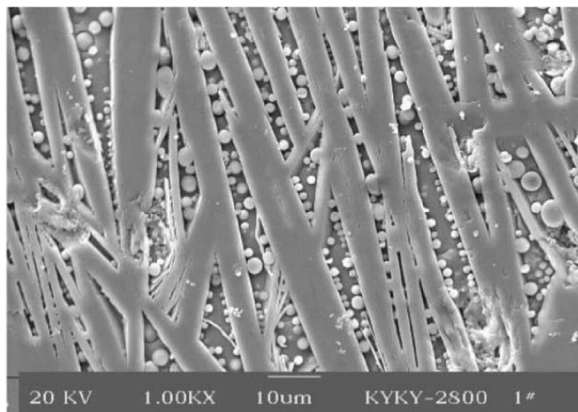


**Fig. 10.** A SEM image showing the dispersion of spherical CaF<sub>2</sub> in inter-plate regions of Al<sub>2</sub>O<sub>3</sub> matrix [55]. (Reprinted from Ref. [55], copyright (2002), with permission from Elsevier).

deposited layers, as compared with Al<sub>2</sub>O<sub>3</sub> substrate.

#### 4.1.2. Biomedical applications

In biomedical industries, not only enhanced wear resistance but also biocompatibility is required. To meet these requirements, Xu et al. laser cladded Si<sub>3</sub>N<sub>4</sub> and calcium phosphate tribasic (TCP) bio-ceramic on a Ti6Al4V substrate [84]. Within cladded layers, Si<sub>3</sub>N<sub>4</sub> was non-cytotoxic and could protect the Ti6Al4V substrate from wearing away. The bioresorbability of TCP facilitated fast bone growth and contributed to its integration with bone tissue [85].

#### 4.1.3. Other applications

Besides excellent mechanical and biomedical properties (such as high wear resistance and bioresorbability), ceramics are also characterized by chemical stability. In order to protect heat exchanger tubes from fireside erosion and corrosion, Khanna et al. laser cladded hard WC/Co layers on a substrate by LD-AM process [86].

### 4.2. Ceramic reinforced MMCs

#### 4.2.1. High wear performance applications

Ceramic materials used for laser cladding are very limited since defects of delamination (i.e. poor bonding) are easily formed especially between the first deposited layer and the substrate. Facing to this problem, researchers have been focused on employing ceramic reinforced MMCs as cladding materials. In ceramic reinforced MMCs, hard ceramic reinforcements in the matrix function as load bearing portion, which can restrain plastic deformation and prevent matrix material from wearing away. The detailed enhancement mechanisms can be summarized as: (1) Ceramic reinforcements possess high strength and high stiffness [36]; (2) The wear resistance of fine-grained microstructure (induced by high heating and high solidification rate in LD-AM process) within cladded layers is higher than that of coarse-

grained microstructure within substrates. [45]. Man et al. in-situ cladded a TiN reinforced MMC layer on a NiTi substrate by LD-AM in a nitrogen atmosphere [5]. Results showed that the wear resistance of NiTi substrate was increased by a factor of two. In order to take the advantages possessed by TiB and TiN, Das et al. in situ synthesized TiB + TiN reinforced TMC on a Ti substrate by LD-AM using premixed BN powder and Ti6Al4V powder [87]. The fine TiB and TiN reinforcements were homogeneously distributed among Ti matrix, remarkably improving wear resistance of the Ti substrate. Van Acker et al. laser cladded WC/W<sub>2</sub>C reinforced NMC composites on steel substrates using LD-AM and investigated effects of WC/W<sub>2</sub>C content as well as carbide size on wear performance [88]. It was evidenced that an increase in WC/W<sub>2</sub>C content and a decrease in carbide size favored the enhancement of wear resistance. In addition, a small amount of carbides was sufficient enough to significantly improve wear resistance. In Wang et al.'s work, in-situ formed TiC reinforced Fe matrix composite (FMC) layers were cladded on a steel substrate, tremendously increasing the wear resistance of steel substrate [89]. Under more demanding conditions (e.g. dry friction with high contact loads) in heavy industry and aerospace areas, both high wear resistance and low friction coefficient are desired. In other words, high wear resistance alone will not satisfy requirements. In response to this problem, Smurov et al. developed two types of cladding structures using LD-AM process, as shown in Fig. 11 [90]. For the first structure (in Fig. 11(a)), ceramic reinforcement of WC/Co and solid lubricant of CuSn comprised deposited layer. Similar to the first structure, the second structure (in Fig. 11(b)) also contained WC/Co reinforced CuSn matrix composite. Besides, the deposited layer of the second structure had hard bars with certain spaces between the bars. The hard bars were made of Stellite and acted as barriers against fast moving of deposited layer and crack propagation when external force was applied. Based on experimental results, both structures demonstrated high wear resistance as well as low friction coefficient.

#### 4.2.2. Biomedical applications

The capability of high load bearing and excellent wear resistance of ceramic reinforced MMCs enable them to find applications in implants with minimized wear induced osteolysis and aseptic loosening [91]. Compared with other types of ceramic reinforced MMCs, ceramic reinforced TMCs (such as TiN reinforced TMC [92] and SiC reinforced TMC [93]) possess high biocompatibility, therefore, they are widely used as cladding layers on metallic substrates to enable or improve the applicability of metallic substrates to biomedical areas. In vitro biocompatibility study, these cladding layers exhibited excellent cell-material interactions and no toxicity and showed their high potential as articular surfaces for load bearing implants, such as hip, knee, and shoulder.

#### 4.2.3. Other applications

Wang et al. successfully fabricated Ni<sub>2</sub>Si/NiSi nickel silicide composite onto a steel substrate by LD-AM process [3]. The cladded layer demonstrated outstanding chemical and electrochemical corrosion resistance under immersion and anodic polarization corrosion test. To improve the slurry erosion wear rate, Tucker et al. laser cladded a

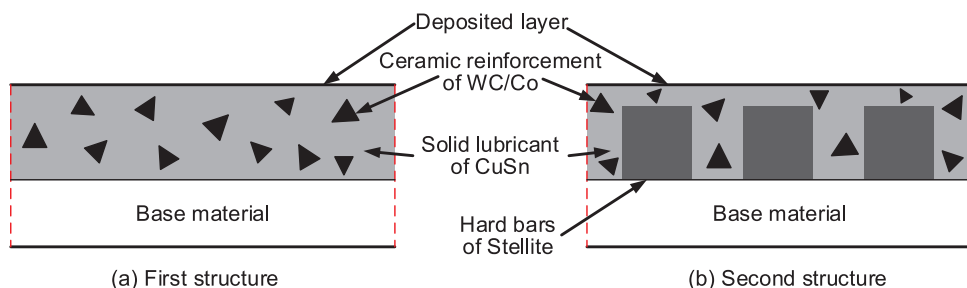


**Fig. 11.** Schematic illustration of two types of LD-AM fabricated structures with high wear resistance and low friction coefficient.

variety of novel composite layers (including TiC reinforced Stellite 6 matrix composites, WC reinforced cobalt matrix composites, MoSi<sub>2</sub> reinforced Stellite 6 matrix composites, and MoSi<sub>2</sub> reinforced steel matrix composites) onto a metal substrate [6]. The effects of composite species and volume fraction of ceramic on the composites were investigated.

## 5. Existing main issues, corresponding solutions, and trend of development

### 5.1. Poor bonding problem in bulk parts fabrication and cladding

In general, ceramic materials are hard to be bonded to metallic substrates. One major reason is ascribed to poor compatibility, resulting from distinctions in melting point, coefficient of thermal expansion, Young's modulus, etc., between deposited layers and substrates [45]. In addition, low wettability (the ability of a liquid to maintain contact with a solid surface) between deposited layers and substrates also accounts for such phenomenon and may cause failure of metallurgical bonding formation [94]. *In bulk parts fabrication, if the deposited first several layers are poorly bonded with the substrate, successive layers deposition will lead to an upwarp of these layers, resulting in fabrication failure. In cladding, the deposited layers will be easily worn off from the substrate during usage as a result of poor bonding.* Facing to these problems, methods on improving bonding properties and bonding strength have been extensively explored.

#### 5.1.1. Optimizing process parameters

For the purpose of obtaining desired bonding, it is indispensable to control and optimize process parameters to melt deposited layers onto a substrate. Wu et al. investigated effects of laser power on bonding conditions in LD-AM of VC-Cr<sub>7</sub>C<sub>3</sub> ceramic on a steel substrate [46]. Bonding was successfully formed when laser power was high enough. When laser power was too low, the deposited VC-Cr<sub>7</sub>C<sub>3</sub> ceramic failed to be bonded with the steel substrate. Emamian et al. systematically studied the effects of process parameters (including laser power, scanning speed, and powder feeding rate) on bonding qualities between deposited TiC layers and a steel substrate [47]. Results showed that a certain range of these process parameters for forming a strong bonding existed. Should improper process parameters be selected, partial bonding or even no bonding would be formed.

#### 5.1.2. Adding a buffer layer/functionally gradient composite layers

Adding a buffer layer is proved to be good for improving compatibility between deposited ceramic layers and metallic substrates and renders a firm bonding between them. As shown in Fig. 12, Gao et al. added an Al-Si buffer layer between an Al<sub>2</sub>O<sub>3</sub> layer and an Mg substrate

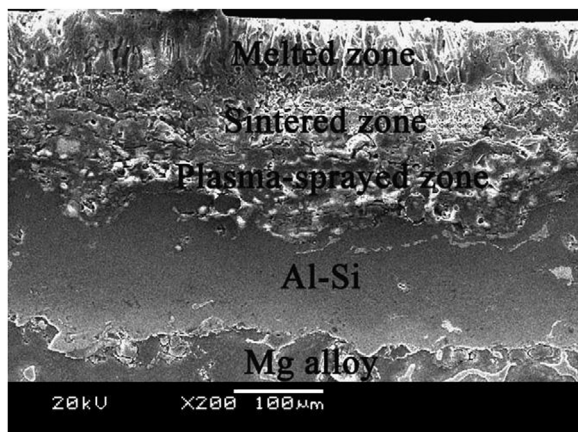


Fig. 12. A cross-section of coating layers observed by SEM imaging [48]. (Reprinted from Ref. [48], copyright (2007), with permission from Elsevier).

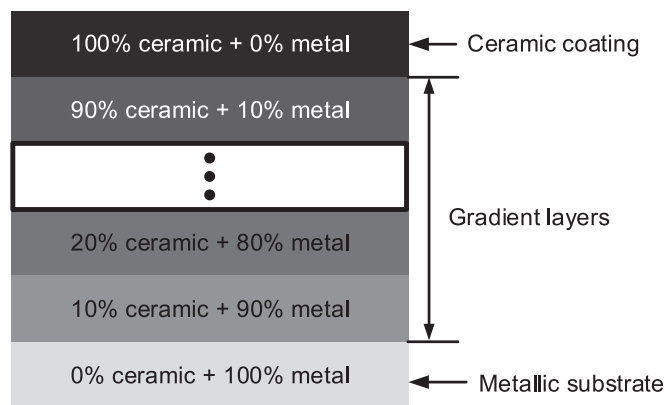


Fig. 13. A structure of step-wise FGC materials.

to release interfacial stresses induced by poor compatibility between them [48]. It was evidenced that bonding interfaces between Al<sub>2</sub>O<sub>3</sub> and Al-Si, Al-Si and Mg were strong and free from obvious defects.

The purpose of using FGC materials is also to provide “buffer layer” between deposited layers and the substrate. The major difference is that in FGC, the “buffer layer” is multi-layers with gradually compositional variation [95]. Fig. 13 shows a typical structure of step-wise FGC layers. By using FGC, the discontinuity of properties between deposited layers and the substrate can be reduced, therefore improving compatibilities between adjacent layers. Balla et al. successfully laser cladded functionally gradient yttria-stabilized ZrO<sub>2</sub> layers on a stainless steel substrate using LD-AM [42]. In LD-AM process, it was proved that the coatings with FGC layers exhibited better bonding strength with the steel substrate than those without FGC layers. In medical field, the utilization of FGC was also proved to be effective of creating sound bonding between ceramic coatings and metallic substrates. Zhu et al. laser cladded bioceramic material, which contained β-tricalcium phosphate and hydroxyapatite, onto a Ti6Al4V substrate [49]. The weight ratio of Ti6Al4V gradually decreased (substrate: 100%; gradient layer 1: 70%; gradient layer 2: 40%; gradient layer 3: 10%; coating layer: 0%) until the bioceramic material dominated the cladded layers. Results showed that the cladded bioceramic layers were chemically and metallurgically bonded with the substrate.

#### 5.1.3. Integrating with assisting technology of ultrasonic vibration

With periodical positive-negative pressures, ultrasonic vibration can give rise to two non-linear actions of acoustic streaming and transient cavitation, as shown in Fig. 14 [2,96–100]. The absorption of acoustic oscillations in liquid materials will generate a steady flow, which is known as acoustic streaming. Transient cavitation involves the formation, growth, pulsation, and collapse of micro-sized bubbles in liquid materials. These two non-linear actions facilitate material movements in liquid and render direct and ultimate influences, which are beneficial for homogenizing material dispersion, smoothing out thermal gradient and thermal stress, reducing cracks, refining grains, etc. [2,98–101]. Therefore, ultrasonic vibration is considered as a potential technology for enhancing bonding strength. Wu et al. deposited a Y<sub>2</sub>O<sub>3</sub> stabilized ZrO<sub>2</sub> layer onto a Ti6Al4V substrate using LD-AM without and with ultrasonic vibration, respectively [50]. By applying ultrasonic vibration, the dilution rate (reflecting the mixture degree between the deposited layers and the substrate [102]) was increased and the bonding was dramatically strengthened.

## 5.2. Cracking problem in bulk parts fabrication and cladding

As a rapid solidification process, cracks induced by large thermal gradient are prone to form during LD-AM of brittle ceramic materials [2]. The exhibition of cracks leads to weakened mechanical properties

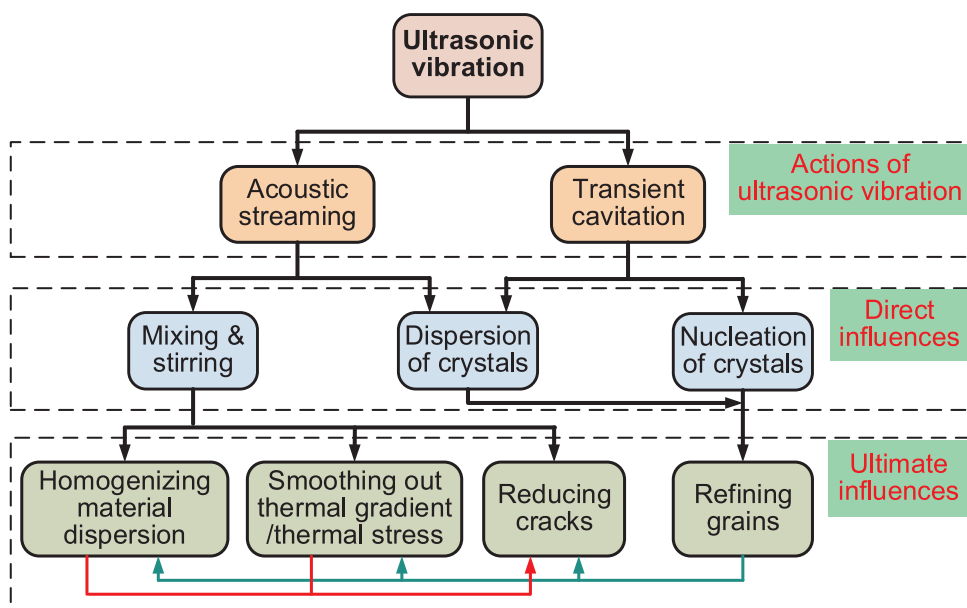


Fig. 14. Actions and influences of ultrasonic vibration in ultrasonic vibration-assisted melting and solidification processes. (After [2,96–100]).

and shortened lifetime of deposited ceramic materials. In addition, the presence of cracks will easily cause the failure of ceramic components or claddings under constant or cyclic loading during operation [103]. In order to improve mechanical properties of the deposited layers as well as to meet the basic demand desired by industries, it is of great importance to suppress cracks and to produce full-dense ceramic parts and claddings.

#### 5.2.1. Optimizing process parameters

Process optimization is a basic and easy-to-control method for researchers to obtain high quality parts and it is applied to suppress cracks in LD-AM process. Hu et al. investigated the effects of laser power on cracking in LD-AM of  $\text{ZrO}_2\text{-Al}_2\text{O}_3$  [2]. As shown in Fig. 15(a), all fabricated parts demonstrated cracks, which initiated at the bottom

and propagated along the build direction. As reported, the tensile stress induced by laser deposition in horizontal direction was larger than that in vertical direction (build direction), leading to cracks propagating along the vertical direction [104]. The tensile stress in the horizontal direction ( $\sigma_H$ ) can be expressed as [104]:

$$\sigma_H = \frac{\pi k E \beta (T_M - T_0) R^2 u}{12 (1-\vartheta) P} \propto \frac{1}{P} \quad (1)$$

where,  $k$  is the thermal conductivity;  $E$  is the Young's modulus;  $\beta$  is the thermal expansion coefficient;  $T_M$  is the melting temperature;  $T_0$  is the environmental temperature;  $R$  is the radius of laser spot;  $\vartheta$  is the Poisson's ratio;  $u$  is the scanning speed;  $P$  is the laser power. It can be concluded from Eq. (1) that when all the other parameters were fixed, the tensile stress in the horizontal direction ( $\sigma_H$ ) had a positive correlation with the inverse of laser power ( $1/P$ ). In other words, high laser power resulted in reduced tensile stress in the horizontal direction, thus decreasing crack propagation degree along build direction. Such tendency was evidenced by experimental results. As shown in Fig. 15(a), the lengths and widths of cracks were hugely reduced by increasing laser power. Niu et al. studied the effects of scanning speed on crack characterizations and concluded that with the scanning speed increasing, both the crack size and crack number were decreased [51]. This was mainly ascribed to the fact that cooling rate would be increased with high scanning speed. High cooling rate rendered fine microstructure, which accounted for decreased crack size and crack number. By optimizing laser power, scanning speed, and powder feeding rate in LD-AM process, Balla et al. fabricated near-full-density  $\text{Al}_2\text{O}_3$  parts, which were almost free from cracks [31].

Although process optimization is an easy-to-control and effective method of reducing cracks, the process parameter window for producing crack-free parts is difficult to find (sometimes even nonexistent) and may involve a large number of experiments [52].

#### 5.2.2. Pre-/post-heating

Pre-heating, the purpose of which is to decrease thermal gradient between deposited materials and a substrate, is proved to be successful of suppressing cracks in LD-AM process [53,54]. Zhou et al. deposited WC reinforced Ni-based matrix composite on a mild steel substrate using LD-AM [53]. By pre-heating the substrate to 900 °C, the deposited composite layers were free from cracks and were metallurgically bonded with the substrate. Meanwhile, the deposition efficiency with

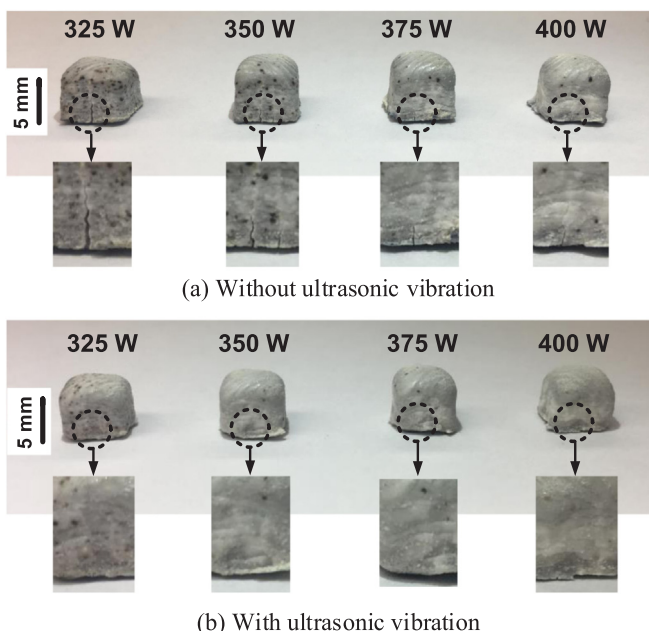


Fig. 15. Effects of ultrasonic vibration on crack suppression under different levels of laser power. (Reprinted from Ref. [2], copyright (2018), with permission from Elsevier).

pre-heating was increased four times higher than that without pre-heating. Liu et al. employed the LD-AM process for fabrication of carbide reinforced TiAl matrix composites on a Ti6Al4V substrate, which was preheated to 450–500 °C. Results showed that the bulk parts fabricated had no cracks [54]. In addition to pre-heating an Al<sub>2</sub>O<sub>3</sub> substrate before depositing CaF<sub>2</sub>/Al<sub>2</sub>O<sub>3</sub> ceramic onto it, Wang et al. also cooled down the substrate slowly on a hot plate after depositing to avoid cracks [55]. For the purpose of healing cracks those already existed, Balla et al. post-heated LD-AM fabricated Al<sub>2</sub>O<sub>3</sub> parts at 1000 °C and 1600 °C. After post-heating, not only the cracks were reduced, but also the density was increased from 94% to 98% and the compressive strength was remarkably improved [31].

In general, pre-/post-heating treatments are time- and cost-consuming since additional procedures and equipment are required. In addition, pre-/post-heating treatments may change desired properties or even damage LD-AM fabricated parts [105].

### 5.2.3. Adding additive materials

Rare earth oxides (REOs), which can change the dynamics of molten pool, are reported to be capable of preventing crack initiation and crack propagation via inhibiting dislocation movements [45,58,106]. Li et al. investigated effects of Y<sub>2</sub>O<sub>3</sub> on cracking in LD-AM of TiB-TiC reinforced TMC on a Ti6Al4V substrate and concluded that the cracking susceptibility of deposited layers was reduced due to the addition of Y<sub>2</sub>O<sub>3</sub> [56]. One major reason was that the Y element would accelerate the spheroidization of primary phase and then refine the microstructure. In addition, Y element also reduced the activity of carbon and prevented it from moving into and traversing the interface of primary phase. Li et al. deposited NBC reinforced FMC layers on a substrate by LD-AM process and proved that the addition of CeO<sub>2</sub> was resultful in reducing inner defects and cracks [57]. Wu et al. deposited carbide reinforced FMC layers on a metal substrate and evidenced that besides Y<sub>2</sub>O<sub>3</sub> and CeO<sub>2</sub>, the addition of other types of REOs (including La<sub>2</sub>O<sub>3</sub>, Pr<sub>6</sub>O<sub>11</sub>, and Nd<sub>2</sub>O<sub>3</sub>) was also favorable for reducing cracks inside deposited layers [58]. As regarded to near-net-shape bulk parts, Niu et al. successfully suppressed crack formation in LD-AM process by adding Y<sub>2</sub>O<sub>3</sub> into Al<sub>2</sub>O<sub>3</sub> [52].

In addition to REOs, ZrO<sub>2</sub> also has positive influence on crack suppression [59]. Fig. 16(a) and (b) show the photographs of a LD-AM fabricated Al<sub>2</sub>O<sub>3</sub> part and a ZrO<sub>2</sub>-Al<sub>2</sub>O<sub>3</sub> part, respectively. The Al<sub>2</sub>O<sub>3</sub> part had a great number of cracks along the build direction. By adding ZrO<sub>2</sub>, the amount of cracks was remarkably reduced. Besides, the shape of ZrO<sub>2</sub>-Al<sub>2</sub>O<sub>3</sub> part was much better than that of Al<sub>2</sub>O<sub>3</sub> part according to the design. The mixture usage of REOs and ZrO<sub>2</sub>, such as Y<sub>2</sub>O<sub>3</sub> stabilized ZrO<sub>2</sub>, was proved to be even more efficient in suppressing cracks in LD-AM process [1,2].

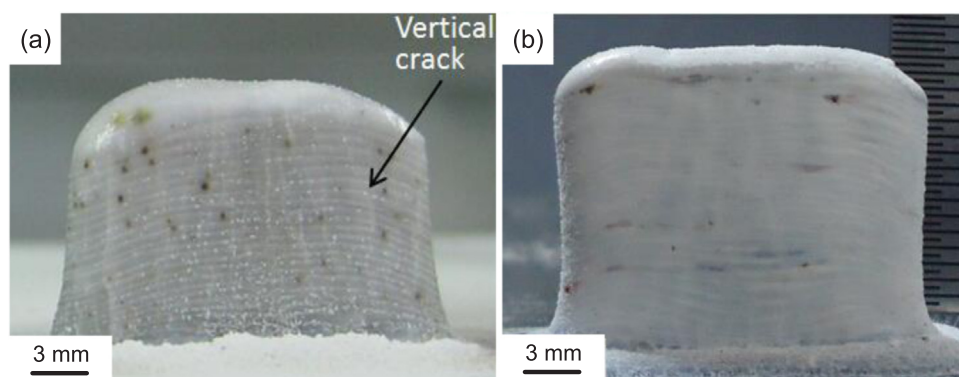


**Fig. 16.** (a) A fabricated Al<sub>2</sub>O<sub>3</sub> part with cracks and a (b) fabricated ZrO<sub>2</sub>-Al<sub>2</sub>O<sub>3</sub> part without cracks [59]. (Reprinted from Ref. [59], copyright (2015), with permission from Emerald Publishing Limited).

### 5.2.4. Integrating with assisting technology of ultrasonic vibration

Due to the advantages exhibited (in Fig. 14), ultrasonic vibration has been introduced and integrated with LD-AM process, aiming at reducing cracks [2,60,61]. Ma et al. deposited Y<sub>2</sub>O<sub>3</sub> stabilized ZrO<sub>2</sub> layers on a Ti alloy substrate [60]. Experimental results showed that the layers deposited with ultrasonic vibration demonstrated refined microstructure, which increased crack propagation energy and inhibited crack propagation. The addition of ultrasonic vibration was also proved to be effective in LD-AM of bulk parts. A novel ultrasonic vibration-assisted LD-AM process for fabrication of ZrO<sub>2</sub>-Al<sub>2</sub>O<sub>3</sub> parts was proposed by Hu et al. [2]. As shown in Fig. 15(b), the parts fabricated with ultrasonic vibration had no cracks. Besides grain refinement, Hu et al. pointed out that the introduction of ultrasonic vibration would contribute to homogenizing material dispersion and smoothing out thermal gradient, thus being beneficial for reducing thermal stress and reducing crack propagation tendency. Such crack suppression phenomenon was also reported by Yan et al. in ultrasonic vibration-assisted LD-AM of eutectic ZrO<sub>2</sub>-Al<sub>2</sub>O<sub>3</sub> parts [61].

### 5.3. Lowered toughness problem in bulk parts fabrication

Despite strengthening effects, ceramic reinforced MMCs suffer severe problems resulted from lowered toughness and ductility due to the presence of rigid ceramic phases [4,30,62]. Therefore, how to strengthen matrix materials without sacrificing too much toughness and ductility becomes an urgent issue which needs to be solved.

#### 5.3.1. Tailoring novel microstructure

It was reported by Attar et al. that the ductility of TiB reinforced TMCs was only one third of that of Ti parts [30]. To reduce this problem, Hu et al. tailored a three-dimensional quasi-continuous network (3DQCN) microstructure within TiB reinforced TMCs using LD-AM [62]. Fig. 17 shows a stereo corner image taken from a fabricated part and corresponding microstructures on each side of the corner. The bright regions and dark regions were identified as TiB reinforcement and Ti matrix, respectively. As reported, the TiB regions were beneficial for strengthening the composites and the Ti regions were able to improve the toughness and ductility of composites [4,62,107]. In addition, the 3D structure could enable uniform load transferring and distributing.

Similar network microstructure was reported in LD-AM of ZrO<sub>2</sub>-Al<sub>2</sub>O<sub>3</sub> [2]. Due to the structural incompatibility between ZrO<sub>2</sub> and Al<sub>2</sub>O<sub>3</sub>, ZrO<sub>2</sub> was expelled and pushed to the boundaries of Al<sub>2</sub>O<sub>3</sub> matrix. At these boundaries, ZrO<sub>2</sub> grew and connected with the formation of a network microstructure, as shown in Fig. 18(a). Element analysis on the network microstructure was conducted with energy-dispersive X-ray spectroscopy (EDXS) mapping, proving that the Al element (representing Al<sub>2</sub>O<sub>3</sub>) was rich at the matrix (in Fig. 18(b)) whereas the Zr

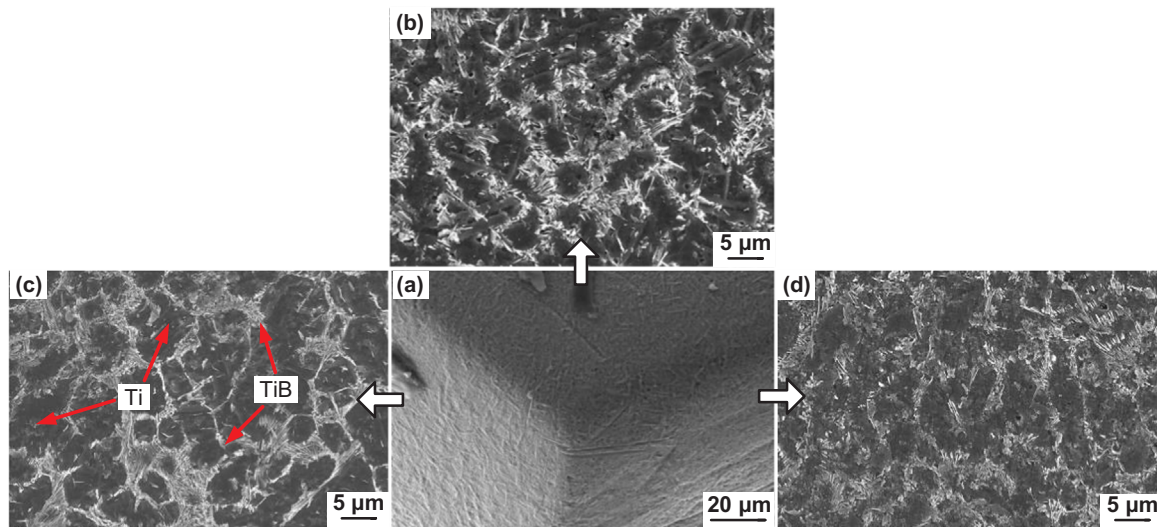


**Fig. 17.** 3DQCN microstructure within TiB reinforced TMCs fabricated by LD-AM process. (a) A stereo corner of a part; Detailed microstructures of (b) top side, (c) left side, and (d) right side. (Reprinted from Ref. [62], copyright (2017), with permission from Elsevier).

element (representing  $ZrO_2$ ) was rich at the boundaries (in Fig. 18(c)). This network microstructure was beneficial for toughening  $Al_2O_3$  matrix through crack bridging, crack deflecting, and crack branching. Toughening mechanisms and crack propagation in the  $ZrO_2$ - $Al_2O_3$  part are shown in Fig. 19. The propagation of initial main crack was blocked by the  $ZrO_2$  phase and a new crack was generated on the other side of the  $ZrO_2$ . This phenomenon, known as crack bridging, could reduce the driving force of cracking and increase the energy required for crack propagation. As the newly generated crack continued propagating, its tip was blunted and deflected by  $ZrO_2$  (crack deflecting) and the crack was branched into two cracks (crack branching). Due to the fact that additional energy was required for deflecting and branching the crack, the  $Al_2O_3$  matrix was toughened [108].

### 5.3.2. Integrating with assisting technology of ultrasonic vibration

As discussed in Section 5.2.3, the  $ZrO_2$  at boundaries could impede crack propagation and then toughened  $Al_2O_3$  matrix. It was confirmed by Hu et al. that the introduction of ultrasonic vibration could further toughen  $Al_2O_3$  matrix in LD-AM fabricated  $ZrO_2$ - $Al_2O_3$  [2]. In comparison with the part fabricated without ultrasonic vibration, an increment of 60% in ultimate compressive strength and an increment of 15% in ductility were achieved by introducing ultrasonic vibration to LD-AM process, as shown in Fig. 20. In addition, the area under the true stress-strain curve (i.e. toughness) of the part fabricated with ultrasonic vibration was larger than that fabricated without ultrasonic vibration. The major reasons for such phenomena were summarized as: (1) The introduction of ultrasonic vibration could reduce thermal stress and inhibit crack propagation, therefore, the energy required for breaking the part was increased and the part was toughened; (2) The total length

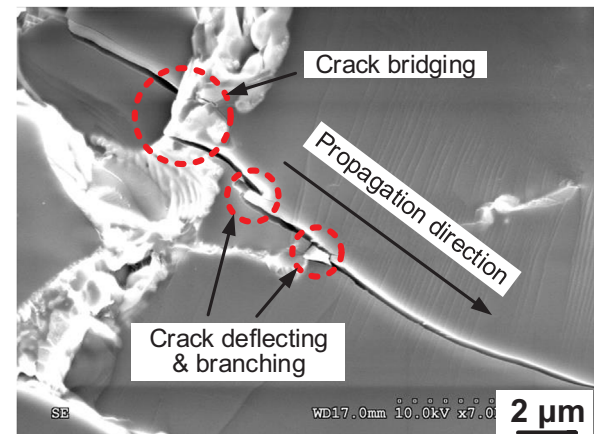


**Fig. 19.** Toughening mechanisms and crack propagation in a  $ZrO_2$ - $Al_2O_3$  part. (Reprinted from Ref. [2], copyright (2018), with permission from Elsevier).

of cracks upon fracture was elongated due to the homogenization of material dispersion caused by ultrasonic vibration; (3) The introduction of ultrasonic vibration would render grain refinement and raise the chance of crack bridging, crack deflecting, and crack branching, thus further toughening  $Al_2O_3$  matrix [2].

## 6. Concluding remarks

In this paper, the research status on LD-AM of ceramics and ceramic

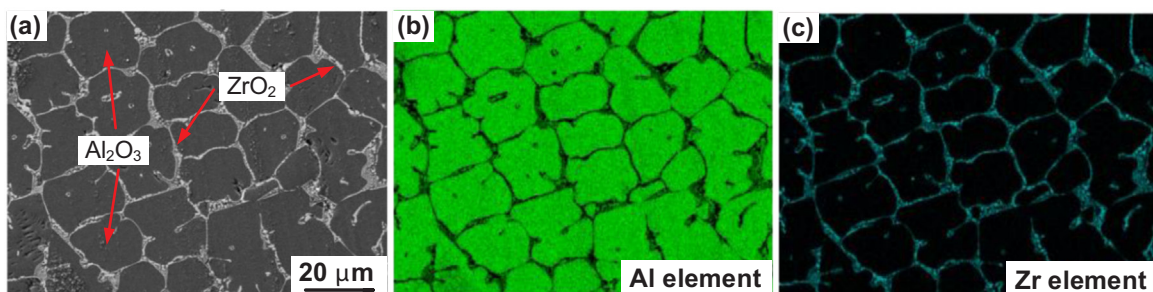


**Fig. 18.** (a) A SEM image on cross-section of a  $ZrO_2$ - $Al_2O_3$  part; (b) and (c) Element analysis on cross-section of the part by EDXS mapping. (Reprinted from Ref. [2], copyright (2018), with permission from Elsevier).

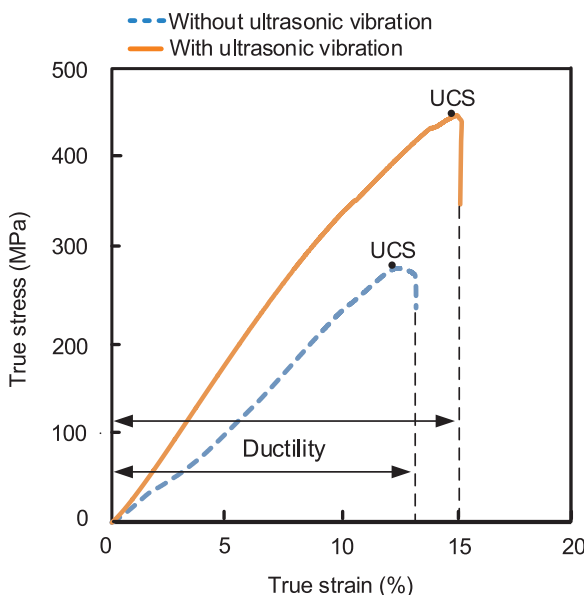


**Fig. 20.** Effects of ultrasonic vibration on compressive properties of the parts fabricated by LD-AM process. (Reprinted from Ref. [2], copyright (2018), with permission from Elsevier).

reinforced MMCs has been reviewed. The main conclusions are drawn as follows:

- (1) The effects of process parameters (e.g. laser power, scanning speed, Z-axis increment, scanning pattern, etc.) in LD-AM have been reviewed, indicating that a proper selection of process parameters contributes to increasing melting degree and uniformizing properties of fabricated parts. In addition, side effects of high thermal stress and part distortion can be reduced or even eliminated by process optimization.
- (2) Equipped with high-power-density laser beams, LD-AM process demonstrates its feasibilities of processing high hardness and high-melting-point ceramics and ceramic reinforced MMCs, such as  $\text{Al}_2\text{O}_3$ ,  $\text{ZrO}_2\text{-Al}_2\text{O}_3$ , TMCs, NMCs, etc. Another important application field of LD-AM process is to clad layers on surfaces of bulk materials with purposes of enhancing surface properties or bringing biological or chemical characteristics to the materials, which will be used in aerospace, biomedical, chemical, electrochemical industries.
- (3) In LD-AM process, strong bonding between deposited ceramics/ceramic reinforced MMC layers and the substrate is of great importance *not only for bulk parts fabrication but also for cladding*. To obtain desired bonding strength, researchers usually start with optimizing process parameters. In situations where process optimization fails to work, adding a buffer layer/FGC layers and integrating with assisting technology of ultrasonic vibration will be good alternatives for forming a firm bonding between deposited layers and the substrate.
- (4) As regard to LD-AM-deposited ceramic materials, cracks caused by large thermal gradient are prone to form. Such problem is detrimental since the exhibition of cracks *will give rise to weakened mechanical properties and shortened lifetime of fabricated bulk parts and claddings*. By optimizing process parameters, the cracking problem can be reduced but cannot be completely eliminated. Besides process optimization, methods of pre-heating the substrate prior to LD-AM process, post-heating the deposited materials to heal existed cracks, adding additive materials (e.g. REOs,  $\text{ZrO}_2$ , etc.), and integrating LD-AM with assisting technology of ultrasonic vibration are also proposed and proved to be successful in suppressing cracks.
- (5) Due to the presence of rigid ceramic phases, LD-AM-fabricated ceramics and ceramic reinforced MMCs suffer severe problems resulted from lowered toughness and ductility. Such issue was alleviated by tailoring innovative 3DQCN microstructures within the fabricated parts and by integrating LD-AM process with ultrasonic vibration.

## References

- [1] F.Y. Niu, D.J. Wu, G.Y. Ma, J.T. Wang, M.H. Guo, B. Zhang, Nanosized microstructure of  $\text{Al}_2\text{O}_3\text{-ZrO}_2$  ( $\text{Y}_2\text{O}_3$ ) eutectics fabricated by laser engineered net shaping, *Scr. Mater.* 95 (2015) 39–41.
- [2] Y.B. Hu, F.D. Ning, W.L. Cong, Y.C. Li, X.L. Wang, H. Wang, Ultrasonic vibration-assisted laser engineered net shaping of  $\text{ZrO}_2\text{-Al}_2\text{O}_3$  bulk parts: effects on crack suppression, microstructure, and mechanical properties, *Ceram. Int.* 44 (3) (2018) 2752–2760.
- [3] H.M. Wang, C.M. Wang, L.X. Cai, Wear and corrosion resistance of laser clad  $\text{Ni}_3\text{Si}/\text{NiSi}$  composite coatings, *Surf. Coat. Technol.* 168 (2) (2003) 202–208.
- [4] Y.B. Hu, W.L. Cong, X.L. Wang, Y.C. Li, F.D. Ning, H. Wang, Laser deposition-additive manufacturing of TiB-Ti composites with novel three-dimensional quasi-continuous network microstructure: effects on strengthening and toughening, *Compos. Part B: Eng.* 133 (2018) 91–100.
- [5] H.C. Man, S. Zhang, F.T. Cheng, X. Guo, In situ formation of a TiN/Ti metal matrix composite gradient coating on NiTi by laser cladding and nitriding, *Surf. Coat. Technol.* 200 (16) (2006) 4961–4966.
- [6] T.R. Tucker, A.H. Clauer, I.G. Wright, J.T. Stropki, Laser-processed composite metal cladding for slurry erosion resistance, *Thin Solid Films* 118 (1) (1984) 73–84.
- [7] J.E. Nevelos, E. Ingham, C. Doyle, A.B. Nevelos, J. Fisher, The influence of acetabular cup angle on the wear of "BIOLOX Forte" alumina ceramic bearing couples in a hip joint simulator, *J. Mater. Sci.: Mater. Med.* 12 (2) (2001) 141–144.
- [8] W. Höland, M. Schweiger, R. Watzke, A. Peschke, H. Kappert, Ceramics as biomaterials for dental restoration, *Expert Rev. Med. Devices* 5 (6) (2008) 729–745.
- [9] D.B. Miracle, Metal matrix composites—from science to technological significance, *Compos. Sci. Technol.* 65 (15–16) (2005) 2526–2540.
- [10] A.D. Kurtz, J.R. Mallon Jr, T.A. Nunn, U.S. Patent No. 4,481,497, U.S. Patent and Trademark Office, Washington, DC, 1984.
- [11] N. Mandal, B. Doloi, B. Mondal, Predictive modeling of surface roughness in high speed machining of AISI 4340 steel using yttria stabilized zirconia toughened alumina turning insert, *Int. J. Refract. Met. Hard Mater.* 38 (2013) 40–46.
- [12] X. He, Y.Z. Zhang, J.P. Mansell, B. Su, Zirconia toughened alumina ceramic foams for potential bone graft applications: fabrication, bioactivation, and cellular responses, *J. Mater. Sci.: Mater. Med.* 19 (7) (2008) 2743–2749.
- [13] N.P. Bansal, A.R. Boccaccini (Eds.), *Ceramics and Composites Processing Methods*, John Wiley & Sons, Hoboken, NJ, 2012.
- [14] W.M. Zeng, Z.C. Li, Z.J. Pei, C. Treadwell, Experimental observation of tool wear in rotary ultrasonic machining of advanced ceramics, *Int. J. Mach. Tools Manuf.* 45 (12–13) (2005) 1468–1473.
- [15] M. Rosso, Ceramic and metal matrix composites: routes and properties, *J. Mater. Process. Technol.* 175 (1–3) (2006) 364–375.
- [16] B. Zhang, X.L. Zheng, H. Tokura, M. Yoshikawa, Grinding induced damage in ceramics, *J. Mater. Process. Technol.* 132 (1–3) (2003) 353–364.
- [17] A. Bandyopadhyay, R.K. Panda, T.F. McNulty, F. Mohammadi, S.C. Danforth, A. Safari, Piezoelectric ceramics and composites via rapid prototyping techniques, *Rapid Prototyp. J.* 4 (1) (1998) 37–49.
- [18] A. Bandyopadhyay, R. Atisivan, G. Kuhn, S. Yeruva, Mechanical properties of interconnected phase alumina-Al composites, in: Proceedings of the Pro SFF, 2000, pp. 24–31.
- [19] T. Chartier, C. Chaput, F. Doreau, M. Loiseau, Stereolithography of structural complex ceramic parts, *J. Mater. Sci.* 37 (15) (2002) 3141–3147.
- [20] C.E. Corcione, A. Greco, F. Montagna, A. Licciulli, A. Maffezzoli, Silica moulds built by stereolithography, *J. Mater. Sci.* 40 (18) (2005) 4899–4904.
- [21] S. Corbel, O. Dufaud, T. Roques-Carmes, Materials for stereolithography, in: Paulo Jorge Bartolo (Ed.), *Stereolithography*, Springer, Boston, MA, 2011, pp. 141–159.
- [22] J. Ebert, E. Özkol, A. Zeichner, K. Übel, Ö. Weiss, U. Koops, R. Telle, H. Fischer, Direct inkjet printing of dental prostheses made of zirconia, *J. Dent. Res.* 88 (7) (2009) 673–676.
- [23] A.M. Waetjen, D.A. Polsakiewicz, I. Kuhl, R. Telle, H. Fischer, Slurry deposition by airbrush for selective laser sintering of ceramic components, *J. Eur. Ceram. Soc.* 29 (1) (2009) 1–6.
- [24] U. Scheithauer, A. Bergner, E. Schwarzer, H.J. Richter, T. Moritz, Studies on thermoplastic 3D printing of steel-zirconia composites, *J. Mater. Res.* 29 (17) (2014) 1931–1940.
- [25] D.A. Klosterman, R.P. Chartoff, N.R. Osborne, G.A. Graves, A. Lightman, G. Han, A. Bezeredi, S. Rodrigues, Development of a curved layer LOM process for monolithic ceramics and ceramic matrix composites, *Rapid Prototyp. J.* 5 (2) (1999) 61–71.
- [26] Y.M. Zhang, J.C. Han, X.H. Zhang, X.D. He, Z.Q. Li, S.Y. Du, Rapid prototyping and combustion synthesis of TiC/Ni functionally graded materials, *Mater. Sci. Eng.: A* 299 (1–2) (2001) 218–224.
- [27] P. Bertrand, F. Bayle, C. Combe, P. Goeriot, I. Smurov, Ceramic components manufacturing by selective laser sintering, *Appl. Surf. Sci.* 254 (4) (2007) 989–992.
- [28] S.K. Ghosh, P. Saha, Crack and wear behavior of SiC particulate reinforced

- aluminium based metal matrix composite fabricated by direct metal laser sintering process, *Mater. Des.* 32 (1) (2011) 139–145.
- [29] J. Wilkes, Y.C. Hagedorn, W. Meiners, K. Wissenbach, Additive manufacturing of  $ZrO_2$ - $Al_2O_3$  ceramic components by selective laser melting, *Rapid Prototyp. J.* 19 (1) (2013) 51–57.
- [30] H. Attar, M. Bönisch, M. Calin, L.C. Zhang, S. Scudino, J. Eckert, Selective laser melting of in situ titanium-titanium boride composites: processing, microstructure and mechanical properties, *Acta Mater.* 76 (2014) 13–22.
- [31] V.K. Balla, S. Bose, A. Bandyopadhyay, Processing of bulk alumina ceramics using laser engineered net shaping, *Int. J. Appl. Ceram. Technol.* 5 (3) (2008) 234–242.
- [32] T. Borkar, S. Gopagni, S. Nag, J.Y. Hwang, P.C. Collins, R. Banerjee, In situ nitridation of titanium-molybdenum alloys during laser deposition, *J. Mater. Sci.* 47 (20) (2012) 7157–7166.
- [33] ASTM, Standard Terminology for Additive Manufacturing Technologies (F-2792-12a), (2015).
- [34] S.H. Huang, P. Liu, A. Mokasdar, L. Hou, Additive manufacturing and its societal impact: a literature review, *Int. J. Adv. Manuf. Technol.* 67 (2013) 1191–1203.
- [35] F.D. Ning, W.L. Cong, Y.B. Hu, H. Wang, Additive manufacturing of carbon fiber-reinforced plastic composites using fused deposition modeling: effects of process parameters on tensile properties, *J. Compos. Mater.* 51 (4) (2017) 451–462.
- [36] Y.B. Hu, F.D. Ning, H. Wang, W.L. Cong, B. Zhao, Laser engineered net shaping of quasi-continuous network microstructural TiB reinforced titanium matrix bulk composites: microstructure and wear performance, *Opt. Laser Technol.* 99 (2018) 174–183.
- [37] Y.Z. Li, Y.B. Hu, W.L. Cong, L. Zhi, Z.N. Guo, Additive manufacturing of alumina using laser engineered net shaping: effects of deposition variables, *Ceram. Int.* 43 (10) (2017) 7768–7775.
- [38] H. Lee, C.H.J. Lim, M.J. Low, N. Tham, V.M. Murukeshan, Y.J. Kim, Lasers in additive manufacturing: a review, *Int. J. Precis. Eng. Manuf.-Green Technol.* 4 (3) (2017) 307–322.
- [39] J.P. Kruth, G. Levy, F. Klocke, T.H.C. Childs, Consolidation phenomena in laser and powder-bed based layered manufacturing, *CIRP Ann.* 56 (2) (2007) 730–759.
- [40] Y.B. Hu, J.Z. Li, Selective laser alloying of elemental titanium and boron powder: thermal models and experiment verification, *J. Mater. Process. Technol.* 249 (2017) 426–432.
- [41] D.D. Gu, W. Meiners, K. Wissenbach, R. Poprawe, Laser additive manufacturing of metallic components: materials, processes and mechanisms, *Int. Mater. Rev.* 57 (3) (2012) 133–164.
- [42] V.K. Balla, P.P. Bandyopadhyay, S. Bose, A. Bandyopadhyay, Compositationally graded yttria-stabilized zirconia coating on stainless steel using laser engineered net shaping (LENS™), *Scr. Mater.* 57 (9) (2007) 861–864.
- [43] Y.B. Hu, H. Wang, F.D. Ning, W.L. Cong, Laser engineered net shaping of commercially pure titanium: effects of fabricating variables, in: Proceedings of the ASME 2016 International Manufacturing Science and Engineering Conference (MSEC2016-8812), Blacksburg, Virginia, USA, 2016. <<http://dx.doi.org/10.1115/MSEC2016-8812>>.
- [44] Optomec, LENS® for 3D printed metals, 2018. Retrieved from <<https://www.optomec.com/>>.
- [45] F. Weng, C.Z. Chen, H.J. Yu, Research status of laser cladding on titanium and its alloys: a review, *Mater. Des.* 58 (2014) 412–425.
- [46] Q.L. Wu, W.G. Li, N. Zhong, W. Gang, W. Haishan, Microstructure and wear behavior of laser cladding VC-Cr<sub>x</sub>C<sub>y</sub> ceramic coating on steel substrate, *Mater. Des.* 49 (2013) 10–18.
- [47] A. Emamian, S.F. Corbin, A. Khajepour, Effect of laser cladding process parameters on clad quality and in-situ formed microstructure of Fe-TiC composite coatings, *Surf. Coat. Technol.* 205 (7) (2010) 2007–2015.
- [48] Y.L. Gao, C.S. Wang, M. Yao, H.B. Liu, The resistance to wear and corrosion of laser-cladding  $Al_2O_3$  ceramic coating on Mg alloy, *Appl. Surf. Sci.* 253 (12) (2007) 5306–5311.
- [49] W.D. Zhu, Q.B. Liu, M. Zheng, X.D. Wang, Biocompatibility of a functionally graded bioceramic coating made by wide-band laser cladding, *J. Biomed. Mater. Res. Part A* 87 (2) (2008) 429–433.
- [50] D.J. Wu, M.H. Guo, G.Y. Ma, F.Y. Niu, Dilution characteristics of ultrasonic assisted laser clad yttria-stabilized zirconia coating, *Mater. Lett.* 141 (2015) 207–209.
- [51] F.Y. Niu, D.J. Wu, S. Yan, G.Y. Ma, B. Zhang, Process optimization for suppressing cracks in laser engineered net shaping of  $Al_2O_3$  ceramics, *JOM* 69 (3) (2016) 557–562.
- [52] F.Y. Niu, D.J. Wu, S.Y. Zhou, G.Y. Ma, Power prediction for laser engineered net shaping of  $Al_2O_3$  ceramic parts, *J. Eur. Ceram. Soc.* 34 (15) (2014) 3811–3817.
- [53] S. Zhou, Y. Huang, X. Zeng, Q. Hu, Microstructure characteristics of Ni-based WC composite coatings by laser induction hybrid rapid cladding, *Mater. Sci. Eng.: A* 480 (1) (2008) 564–572.
- [54] W.P. Liu, J.N. DuPont, Fabrication of carbide-particle-reinforced titanium aluminide-matrix composites by laser-engineered net shaping, *Metall. Mater. Trans. A* 35 (3) (2004) 1133–1140.
- [55] H.M. Wang, Y.L. Yu, S.Q. Li, Microstructure and tribological properties of laser clad  $CaF_2$ - $Al_2O_3$  self-lubrication wear-resistant ceramic matrix composite coatings, *Scr. Mater.* 47 (1) (2002) 57–61.
- [56] J. Li, X. Luo, G.J. Li, Effect of  $Y_2O_3$  on the sliding wear resistance of TiB/TiC-reinforced composite coatings fabricated by laser cladding, *Wear* 310 (1–2) (2014) 72–82.
- [57] Q.T. Li, Y.P. Lei, H.G. Fu, Laser cladding in-situ NbC particle reinforced Fe-based composite coatings with rare earth oxide addition, *Surf. Coat. Technol.* 239 (2014) 102–107.
- [58] C.F. Wu, M.X. Ma, W.J. Liu, M.L. Zhong, H.J. Zhang, W.M. Zhang, Laser cladding in-situ carbide particle reinforced Fe-based composite coatings with rare earth oxide addition, *J. Rare Earths* 27 (6) (2009) 997–1002.
- [59] F.Y. Niu, D.J. Wu, G.Y. Ma, S.Y. Zhou, B. Zhang, Effect of second-phase doping on laser deposited  $Al_2O_3$  ceramics, *Rapid Prototyp. J.* 21 (2) (2015) 201–206.
- [60] G.Y. Ma, S. Yan, D.J. Wu, Q.Y. Miao, M.R. Liu, F.Y. Niu, Microstructure evolution and mechanical properties of ultrasonic assisted laser clad yttria stabilized zirconia coating, *Ceram. Int.* 43 (13) (2017) 9622–9629.
- [61] S. Yan, D.J. Wu, F.Y. Niu, G.Y. Ma, R.K. Kang,  $Al_2O_3$ - $ZrO_2$  eutectic ceramic via ultrasonic-assisted laser engineered net shaping, *Ceram. Int.* 43 (17) (2017) 15905–15910.
- [62] Y.B. Hu, B. Zhao, F.D. Ning, H. Wang, W.L. Cong, In-situ ultrafine three-dimensional quasi-continuous network microstructural TiB reinforced titanium matrix composites fabrication using laser engineered net shaping, *Mater. Lett.* 195 (2017) 116–119.
- [63] F.A. España, V.K. Balla, S. Bose, A. Bandyopadhyay, Design and fabrication of CoCrMo alloy based novel structures for load bearing implants using laser engineered net shaping, *Mater. Sci. Eng.: C* 30 (1) (2010) 50–57.
- [64] Y.B. Hu, F.D. Ning, X.L. Wang, H. Wang, B. Zhao, W.L. Cong, Y.Z. Li, Laser deposition-additive manufacturing of in situ TiB reinforced titanium matrix composites: TiB growth and part performance, *Int. J. Adv. Manuf. Technol.* 93 (9–12) (2017) 3409–3418.
- [65] N. Shamsaei, A. Yadollahi, L. Bian, S.M. Thompson, An overview of direct laser deposition for additive manufacturing: part II: mechanical behavior, process parameter optimization and control, *Addit. Manuf.* 8 (2015) 12–35.
- [66] F.Y. Niu, D.J. Wu, G.Y. Ma, B. Zhang, Additive manufacturing of ceramic structures by laser engineered net shaping, *Chin. J. Mech. Eng.* 28 (6) (2015) 1117–1122.
- [67] D.J. Wu, B. Sun, F.Y. Niu, G.Y. Ma, Y.L. Zhang, Z.J. Jin, Microstructure and crack in color  $Al_2O_3$  samples by laser engineered net shaping, *J. Chin. Ceram. Soc.* 41 (12) (2013) 1621–1626.
- [68] D. Gutknecht, J. Chevalier, V. Garnier, G. Fantozzi, Key role of processing to avoid low temperature ageing in alumina zirconia composites for orthopaedic application, *J. Eur. Ceram. Soc.* 27 (2) (2007) 1547–1552.
- [69] I. Ganesh, S.M. Olhero, P.M. Torres, F.J. Alves, J.M. Ferreira, Hydrolysis-induced aqueous gelcasting for near-net shape forming of ZTA ceramic composites, *J. Eur. Ceram. Soc.* 29 (8) (2009) 1393–1401.
- [70] J. Wang, R. Stevens, Zirconia-toughened alumina (ZTA) ceramics, *J. Mater. Sci.* 24 (10) (1989) 3421–3440.
- [71] I. Denry, J.R. Kelly, State of the art of zirconia for dental applications, *Dent. Mater.* 24 (3) (2008) 299–307.
- [72] S.A. Bernard, V.K. Balla, S. Bose, A. Bandyopadhyay, Direct laser processing of bulk lead zirconate titanate ceramics, *Mater. Sci. Eng.: B* 172 (1) (2010) 85–88.
- [73] D. Liu, S.Q. Zhang, A. Li, H.M. Wang, Microstructure and tensile properties of laser melting deposited TiC/TA15 titanium matrix composites, *J. Alloy. Compd.* 485 (1–2) (2009) 156–162.
- [74] R.M. Mahamood, E.T. Akinlabi, M. Shukla, S. Pityana, Scanning velocity influence on microstructure, microhardness and wear resistance performance of laser deposited Ti6Al4V/TiC composite, *Mater. Des.* 50 (2013) 656–666.
- [75] S. Tamirisakandala, D.B. Miracle, R. Srinivasan, J.S. Gunasekera, Titanium alloyed with boron, *Adv. Mater. Process.* 164 (12) (2006) 41.
- [76] B.F. Decker, J.S. Kasper, The crystal structure of TiB, *Acta Crystallogr.* 7 (1) (1954) 77–80.
- [77] W.J. Lu, L. Xiao, K. Geng, J.N. Qin, D. Zhang, Growth mechanism of in situ synthesized TiBw in titanium matrix composites prepared by common casting technique, *Mater. Charact.* 59 (7) (2008) 912–919.
- [78] P. Chandrasekar, V. Balusamy, K.R. Chandran, H. Kumar, Laser surface hardening of titanium-titanium boride (Ti-TiB) metal matrix composite, *Scr. Mater.* 56 (7) (2007) 641–644.
- [79] S. Gopagni, J.Y. Hwang, A.R.P. Singh, B.A. Mensah, N. Bunce, J. Tiley, T.W. Scharf, R. Banerjee, Microstructural evolution in laser deposited nickel-titanium-carbon in situ metal matrix composites, *J. Alloy. Compd.* 509 (4) (2011) 1255–1260.
- [80] C. Hong, D.D. Gu, D.H. Dai, M. Alkhayat, W. Urban, P.P. Yuan, S.N. Cao, A. Gasser, A. Weisheit, I. Kelbassa, M.L. Zhong, R. Poprawe, Laser additive manufacturing of ultrafine TiC particle reinforced Inconel 625 based composite parts: tailored microstructures and enhanced performance, *Mater. Sci. Eng.: A* 635 (2015) 118–128.
- [81] X.C. Li, J. Stampfli, F.B. Prinz, Mechanical and thermal expansion behavior of laser deposited metal matrix composites of Invar and TiC, *Mater. Sci. Eng.: A* 282 (1) (2000) 86–90.
- [82] I. Watanabe, M. McBride, P. Newton, K.S. Kurtz, Laser surface treatment to improve mechanical properties of cast titanium, *Dent. Mater.* 25 (5) (2009) 629–633.
- [83] J.D. Majumdar, I. Manna (Eds.), *Laser-Assisted Fabrication of Materials*, 161 Springer Science & Business Media, Berlin, Germany, 2012.
- [84] X. Xu, J.G. Han, C.M. Wang, A.G. Huang, Laser cladding of composite bioceramic coatings on titanium alloy, *J. Mater. Eng. Perform.* 25 (2) (2016) 656–667.
- [85] M. Roy, B.V. Krishna, A. Bandyopadhyay, S. Bose, Laser processing of bioactive tricalcium phosphate coating on titanium for load-bearing implants, *Acta Biomater.* 4 (2) (2008) 324–333.
- [86] A.S. Khanna, S. Kumari, S. Kanungo, A. Gasser, Hard coatings based on thermal spray and laser cladding, *Int. J. Refract. Met. Hard Mater.* 27 (2) (2009) 485–491.
- [87] M. Das, V.K. Balla, D. Basu, I. Manna, T.S. Kumar, A. Bandyopadhyay, Laser processing of in situ synthesized TiB-TiN-reinforced Ti6Al4V alloy coatings, *Scr. Mater.* 66 (8) (2012) 578–581.
- [88] K. Van Acker, D. Vanhooyweghen, R. Persoons, J. Vangrunderbeek, Influence of tungsten carbide particle size and distribution on the wear resistance of laser clad WC/Ni coatings, *Wear* 258 (1–4) (2005) 194–202.

- [89] X.H. Wang, M. Zhang, X.M. Liu, S.Y. Qu, Z.D. Zou, Microstructure and wear properties of TiC/FeCrBSi surface composite coating prepared by laser cladding, *Surf. Coat. Technol.* 202 (15) (2008) 3600–3606.
- [90] I. Smurov, Laser cladding and laser assisted direct manufacturing, *Surf. Coat. Technol.* 202 (18) (2008) 4496–4502.
- [91] M. Das, V.K. Balla, T.S. Kumar, I. Manna, Fabrication of biomedical implants using laser engineered net shaping (LENS™), *Trans. Indian Ceram. Soc.* 72 (3) (2013) 169–174.
- [92] V.K. Balla, A. Bhat, S. Bose, A. Bandyopadhyay, Laser processed TiN reinforced Ti6Al4V composite coatings, *J. Mech. Behav. Biomed. Mater.* 6 (2012) 9–20.
- [93] M. Das, V.K. Balla, T.S. Kumar, A. Bandyopadhyay, I. Manna, Tribological, electrochemical and in vitro biocompatibility properties of SiC reinforced composite coatings, *Mater. Des.* 95 (2016) 510–517.
- [94] J.S. Amin, E. Nikoee, S. Ayatollahi, A. Alamdari, Investigating wettability alteration due to asphaltene precipitation: imprints in surface multifractal characteristics, *Appl. Surf. Sci.* 256 (21) (2010) 6466–6472.
- [95] P.P. Bandyopadhyay, V.K. Balla, S. Bose, A. Bandyopadhyay, Compositationally graded aluminum oxide coatings on stainless steel using laser processing, *J. Am. Ceram. Soc.* 90 (7) (2007) 1989–1991.
- [96] Y. Yang, J. Lan, X.C. Li, Study on bulk aluminum matrix nano-composite fabricated by ultrasonic dispersion of nano-sized SiC particles in molten aluminum alloy, *Mater. Sci. Eng.: A* 380 (1–2) (2004) 378–383.
- [97] F.D. Ning, Y.B. Hu, Z.C. Liu, X.L. Wang, Y.Z. Li, W.L. Cong, Ultrasonic vibration-assisted laser engineered net shaping of Inconel 718 parts: microstructural and mechanical characterization, *J. Manuf. Sci. Eng.-Trans. ASME* 140 (6) (2018) 061012.
- [98] O.V. Abramov, Action of high intensity ultrasound on solidifying metal, *Ultrasonics* 25 (2) (1987) 73–82.
- [99] W.L. Cong, F.D. Ning, A fundamental investigation on ultrasonic vibration-assisted laser engineered net shaping of stainless steel, *Int. J. Mach. Tools Manuf.* 121 (2017) 61–69.
- [100] L. Moraru, Ultrasound action on strength properties of polycrystalline metals, 2006.
- [101] F.D. Ning, Y.B. Hu, Z.C. Liu, W.L. Cong, Y.Z. Li, X.L. Wang, Ultrasonic vibration-assisted laser engineered net shaping of Inconel 718 parts: a feasibility study, *Procedia Manuf.* 10 (2017) 771–778.
- [102] E. Toyserkani, A. Khajepour, S.F. Corbin, *Laser Cladding*, CRC press, Boca Raton, FL, 2004.
- [103] D. Munz, T. Fett, *Ceramics: Mechanical Properties, Failure Behavior, Materials Selection* 36 Springer Science & Business Media, Berlin, Germany, 2013.
- [104] D. Triantafyllidis, L. Li, F.H. Stott, Crack-free densification of ceramics by laser surface treatment, *Surf. Coat. Technol.* 201 (6) (2006) 3163–3173.
- [105] S.F. Zhou, X.Y. Zeng, Q.W. Hu, Y.J. Huang, Analysis of crack behavior for Ni-based WC composite coatings by laser cladding and crack-free realization, *Appl. Surf. Sci.* 255 (5) (2008) 1646–1653.
- [106] M.M. Quazi, M.A. Fazal, A.S.M.A. Haseeb, F. Yusof, H.H. Masjuki, A. Arslan, Effect of rare earth elements and their oxides on tribomechanical performance of laser claddings: a review, *J. Rare Earths* 34 (6) (2016) 549–564.
- [107] L.J. Huang, L. Geng, H.X. Peng, Microstructurally inhomogeneous composites: is a homogeneous reinforcement distribution optimal? *Prog. Mater. Sci.* 71 (2015) 93–168.
- [108] S. Zhang, D. Sun, Y.Q. Fu, H.J. Du, Toughening of hard nanostructural thin films: a critical review, *Surf. Coat. Technol.* 198 (1–3) (2005) 2–8.